AGU PUBLICATIONS

JGR

Journal of Geophysical Research: Earth Surface

RESEARCH ARTICLE
10.1002/2013JF002874

Key Points:
- Power laws connect bed load volumes and transport distances with stream power
- Bed load volumes and transport distances are correlated to each other
- Bed load volumes and transport distances allow computation of active layer depth

Supporting Information:
- Readme
- Text S1

Correspondence to:
J. M. Schneider,
johannes.schneider@wsl.ch

Citation:
Schneider, J. M., J. M. Turowski, D. Rickenmann, R. Hegglin, S. Arrigo, L. Mao, and J. W. Kirchner (2014), Scaling relationships between bed load volumes, transport distances, and stream power in steep mountain channels, *J. Geophys. Res. Earth Surf.*, *119*, 533–549, doi:10.1002/2013JF002874.

Received 4 JUN 2013
Accepted 19 JAN 2014
Accepted article online 24 JAN 2014
Published online 13 MAR 2014

Scaling relationships between bed load volumes, transport distances, and stream power in steep mountain channels

Johannes M. Schneider[1,2], Jens M. Turowski[3,1], Dieter Rickenmann[1], Ramon Hegglin[1], Sabrina Arrigo[1], Luca Mao[4], and James W. Kirchner[2,1]

[1]Mountain Hydrology and Mass Movements, Swiss Federal Research Institute WSL, Birmensdorf, Switzerland, [2]Department of Environmental System Science, Swiss Federal Institute of Technology ETH, Zurich, Switzerland, [3]Helmholtz Centre Potsdam, German Research Centre for Geosciences GFZ, Potsdam, Germany, [4]Department of Ecosystems and Environment, Pontificia Universidad Católica de Chile, Santiago, Chile

Abstract Bed load transport during storm events is both an agent of geomorphic change and a significant natural hazard in mountain regions. Thus, predicting bed load transport is a central challenge in fluvial geomorphology and natural hazard risk assessment. Bed load transport during storm events depends on the width and depth of bed scour, as well as the transport distances of individual sediment grains. We traced individual gravels in two steep mountain streams, the Erlenbach (Switzerland) and Rio Cordon (Italy), using magnetic and radio frequency identification tags, and measured their bed load transport rates using calibrated geophone bed load sensors in the Erlenbach and a bed load trap in the Rio Cordon. Tracer transport distances and bed load volumes exhibited approximate power law scaling with both the peak stream power and the cumulative stream energy of individual hydrologic events. Bed load volumes scaled much more steeply with peak stream power and cumulative stream energy than tracer transport distances did, and bed load volumes scaled as roughly the third power of transport distances. These observations imply that large bed load transport events become large primarily by scouring the bed deeper and wider, and only secondarily by transporting the mobilized sediment farther. Using the sediment continuity equation, we can estimate the mean effective thickness of the actively transported layer, averaged over the entire channel width and the duration of individual flow events. This active layer thickness also followed approximate power law scaling with peak stream power and cumulative stream energy and ranged up to 0.57 m in the Erlenbach, broadly consistent with independent measurements.

1. Introduction

Bed load transport during flood events in mountain channels is an important agent of geomorphic change [*Schumm*, 1977] and an important natural hazard which can cause enormous damage in mountainous regions [e.g., *Badoux et al*., 2014]. Estimates of bed load transport typically rely on measurements that require substantial effort and specially designed samplers, possibly involving construction within the streambed (e.g., vortex samplers [*Klingeman*, 1979], Birkbeck samplers [*Reid et al*., 1980], or moving bed load baskets [*Rickenmann et al*., 2012]), or that can be used only in specific locations for short intervals of time (e.g., Helley-Smith samplers or bed load traps [*Helley and Smith*, 1971; *Bunte et al*., 2004]). In unmeasured stream reaches, estimates of transported bed load volumes rely on empirical equations, which are normally developed from limited laboratory and field data and have large predictive uncertainties, especially in mountain streams [e.g., *Bathurst et al*., 1987; *Rickenmann*, 2001; *Nitsche et al*., 2011].

Another approach for estimating bed load transport is based on the notion that the bulk bed load is controlled by individually moving particles. Typically, the movements of individual particles consist of a series of steps and rest periods due to the turbulent flow conditions and irregular bed forms [e.g., *Einstein*, 1937; *Hassan et al*., 1991; *Lajeunesse et al*., 2010]. The sum of those individual particle step lengths during a transport event results in a total transport distance. Information on transport distances (or velocities), combined with information on entrainment rates or dimensions of a mobile layer depth, enables the estimation of bed load volumes (or rates) during a flood event (or observation period) [*Hassan and Ergenzinger*, 2005; *Haschenburger and Church*, 1998; *Houbrechts et al*., 2012; *Laronne et al*., 1992; *Liébault and Laronne*, 2008; *Sear et al*., 2000; *Wilcock*, 1997; *Wong and*

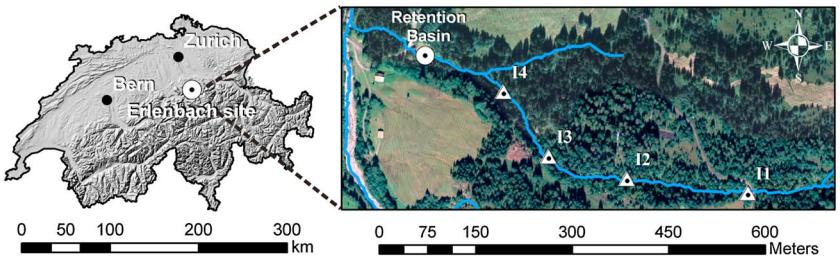

Figure 1. Erlenbach field site in Swiss Pre-Alps, showing tracer insertion points (triangles I1-I4). Maps reproduced from BFS GEOSTAT and swissimage ©2012, swisstopo DV 033594.

Parker, 2006; *Wong et al*., 2007]. To determine total transport distances in natural channels, particles have been traced for individual transport events or longer observations periods using, e.g., color markings, magnetic tracers, or radio frequency identification (RFID) transponders [e.g., *Bunte and Ergenzinger*, 1989; *Gintz et al*., 1996; *Haschenburger and Church*, 1998; *Lamarre and Roy*, 2008; *Lamarre et al*., 2005; *Liébault et al*., 2012; *Schmidt and Ergenzinger*, 1992]. Particle tracking data have been used to constrain transport distance distributions and their dependence on channel morphology or flood magnitude (e.g., the Einstein-Sayre-Hubbel model and gamma or exponential distributions [*Bradley and Tucker*, 2012; *Einstein*, 1937; *Gintz et al*., 1996; *Hassan et al*., 1991, 2013; *Liébault et al*., 2012; *Sayre and Hubbell*, 1964]). However, few studies exist for mountain streams where measured bed load volumes and transport distances of individual particles are available for the same transport events. *Lenzi* [2004] provided data for bed load volumes and transport distances for individual transport events for the Rio Cordon (Italy) while *Liébault and Laronne* [2008] measured the total bed load yield for an entire tracer transport distance campaign in the Escanovette torrent (France). *Houbrechts et al*. [2012] provided measurements of bed load transport and transport distances for several larger and lower gradient rivers in the Ardennes (Belgium).

Understanding how bed load volumes and transport distances scale with one another and with the size of a flood event (as characterized, for example, by the peak flow or the total storm runoff) is important for predicting large transport events and also for understanding how they affect the streambed. To characterize the impact of transport events on the streambed, we use the concept of the active layer [*Hirano*, 1971; *Parker*, 1991; *Parker et al*., 2000], which can be defined as "the portion of the streambed that is mobilized during floods competent to transport sediment" [*Haschenburger and Church*, 1998]. The depth of the active layer may be relevant to fields as diverse as ecology (e.g., excavation of spawning gravels), engineering (e.g., scour of engineered structures in streams), and geomorphology (e.g., as a control on sediment delivery during flood events).

In this study we compiled a distinctive data set on measured transport distances and bed load volumes in two steep mountain streams, the Erlenbach (Switzerland) and Rio Cordon (Italy [*Lenzi et al*., 2004]) for flood events with a broad range of flow magnitudes. We examine how transport distances and bed load volumes scale with the stream power of the peak discharge and the stream energy of the entire flood event and compare our findings with literature results. Based on the transport distance and bed load data, it was possible to back-calculate an active layer depth to estimate the effects of flow events on the streambed.

2. Field Sites and Methods

2.1. Field Sites

2.1.1. Erlenbach

The Erlenbach is a steep mountain stream (mean gradient: 0.17) draining an area of 0.7 km^2 in the Swiss pre-Alps (Figure 1 and Table 1). The runoff regime is nivopluvial (snow and rain dominated) with the largest transport events caused by extreme summer rainstorms. Occasional snowmelt and rain-on-snow events are of secondary importance for sediment transport.

In this study, transport events were observed covering a range of flow magnitudes with peak discharges (Q_p) of 0.5–10 m^3/s. For later analysis, we define transport events with $Q_p < 1.5\ m^3/s$, $1.5 \le Q_p < 3\ m^3/s$, and $Q_p \ge 3\ m^3/s$ as low-, moderate-, and high-magnitude flood events, respectively. The corresponding

Table 1. Main Characteristics of the Erlenbach and Rio Cordon Catchments

	Erlenbach (CH)	Rio Cordon (IT)
Basin elevation range (m)	1110–1655	1763–2748
Basin area (km^2)	0.7	5
Mean slope/slope study reach (m/m)	0.17/0.15	0.13
Mean width (m)	3.5	5.7
Channel type	Step-pool	Step-pool
$D_{25Surf}/D_{50Surf}/D_{84Surf}$[a] (mm)	16/64/206	38/90/262
Lithology	Flysch	Dolomites and volcaniclastic conglomerates
Forested %	39	7
Discharge regime	nivo-pluvial	nivo-pluvial
$RI_2/RI_5/RI_{10}$[b] (m^3/s)	2/4/7	3/5/7
Mean annual precipitation (mm)	2300	1100
Average bed load yield ($m^3\,km^{-2}yr^{-1}$)	~570	~20

[a]Referring to the bed surface sediment.
[b]Flood with recurrence interval (*RI*) of 2, 5, and 10 years [*Liechti*, 2008; *Lenzi et al*., 2004].

recurrence intervals are approximately <1 year, 1–3 years, and >3 years, respectively [*Liechti*, 2008]. Flow discharge at the Erlenbach is measured directly upstream of a sediment retention basin, but because the main part of the Erlenbach tracer study reach was upstream of a small tributary (Figure 1), we reduced the measured discharge proportionally to account for the reduced drainage area.

The Erlenbach stream is characterized by a rough channel bed with a step-pool morphology and large relatively immobile boulders [*Molnar et al*., 2010]. The grain-size distribution (GSD) of the channel bed surface was determined by grid-by-number pebble counts in September 2012 using a variant of the *Wolman* [1954] procedure, according to *Bunte and Abt* [2001a, 2001b] and *Bunte et al*. [2009] (Figure 2). Bed material subsurface GSDs were determined by sieve analysis of three large volumetric samples taken using a three-sided plywood shield [*Bunte and Abt*, 2001b]. The GSDs of the transported bed load were determined by four sieved samples taken in the sediment retention basin from 1984 to 1987 [see also *Rickenmann and McArdell*, 2007]. The characteristic grain sizes $D_{25Surf}/D_{50Surf}/D_{84Surf}$ of the streambed surface were 16/64/206 mm. In this paper, characteristic grain sizes of the streambed surface are subscripted with "Surf," of the streambed subsurface with "Sub," and of the bed load transported to the retention basin with "B," respectively (e.g., D_{50Surf}, D_{50Sub}, and D_{50B}).

2.1.2. Rio Cordon

Rio Cordon is a boulder bed stream draining an area of 5 km^2 in the Italian Alps [see also *Lenzi*, 2004; *Lenzi et al*., 2006; *Mao et al*., 2009, 2010, and references therein], with a mean channel gradient of 0.13. Precipitation occurs mainly as snowfall from November to April and runoff is usually dominated by snowmelt in May and June, but summer and early autumn floods represent an important contribution to the flow regime. The peak discharges of the flood events analyzed during this study range from about 0.8 to 10 m^3/s.

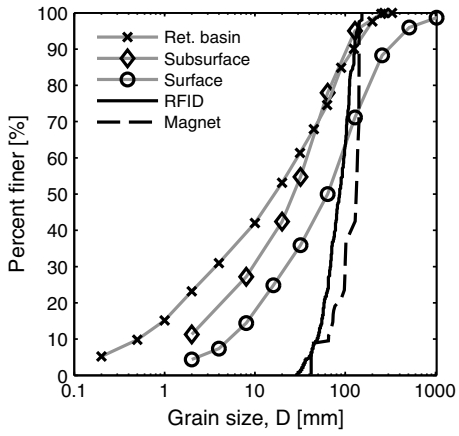

Figure 2. Grain-size distributions of the sediment deposited in the Erlenbach retention basin (crosses), of the channel bed subsurface and surface (diamonds and circles, respectively), and of the RFID and magnetic tracer populations (solid and dotted lines, respectively).

The channel bed consists of step-pool, riffle-pool, and mixed reaches. The characteristic grain sizes of the streambed surface $D_{25Surf}/D_{50Surf}/D_{84Surf}$ were identified by grid-by-number pebble counts as 38/90/262 mm, and the bed surface is strongly armored ($D_{50Surf}/D_{50Sub} \sim 3$) [*Lenzi*, 2004].

2.2. Characterization of Hydraulic Forcing

Bed load transport rates and distances are functions of hydraulic forcing, which in this study is characterized by stream power [*Bagnold*, 1966]. Stream power has been shown to be more reliable than shear stress as a measure of hydraulic forcing [e.g., *Gomez and Church*, 1989; *Rickenmann*, 2001],

Table 2. Tracer Survey Periods at Erlenbach and Recovery Rates[a]

	ID	Period		Q_p (m^3/s)	N_t	N_{EvB}	N_m	P_b (%)	P_t (%)	P_{EvB} (%)	P_{RER} (%)	P_{Lost} (%)
		From	To									
RFID tracer	**1**[b]	11.06.09	18.06.09	3.0	95	95	88	42	31	31	31	38
	2[c]	18.06.09	07.07.09	5.0	81	80	60	42	27	*36*	*26*	38
	3[e]	07.07.09	16.07.09	0.7	106	70	9	39	25	86	10	4
	4	16.07.09	21.07.09	1.3	112	92	14	49	26	87	7	6
	5	21.07.09	26.07.09	1.3	120	102	15	50	28	91	4	5
	6	28.07.09	04.08.09	1.2	125	99	25	42	29	83	7	10
	7	04.08.09	12.08.09	1.3	118	107	22	39	27	86	4	10
	8[b]	18.06.10	22.06.10	0.5	175[f]	166	65	30	50	47	26	27
	9	22.06.10	12.07.10	0.7	109	77	36	11	27	44	35	21
	10[e]	12.07.10	13.07.10	2.4	110	27	22	29	25	25	12	63
	11	13.07.10	19.07.10	0.8	91	70	11	24	21	64	15	21
	12	19.07.10	26.07.10	1.6	93	58	23	45	20	64	4	32
	13[e]	26.07.10	28.07.10	4.7	43	18	11	30	6	19	6	75
	14[e]	28.07.10	01.08.10	1.5	47	32	6	57	6	74	2	24
	15[e]	01.08.10	04.08.10	9.3	16	5	3	44	2	11	4	85
	16[e]	04.08.10	11.08.11	2.4	15	9	4	40	1	56	6	38
Magnetic tracer	**17**[b]	18.07.94	25.08.94	2.0	159	159	112	-	30	51	15	34
	18[d]	25.08.94	21.09.94	1.6	121	115	73	-	39	72	8	20
	19[d]	29.11.94	26.06.95	1.0	108	95	101	-	35	76	1	23
	20	26.06.95	28.07.95	10.0	40	26	27	-	13	24	0	76
	21[b,d]	22.05.97	30.07.97	1.4	174	174	155	-	77	77	5	18
	22[e]	30.07.97	26.08.97	0.9	154	153	6	-	68	88	2	10
	23[e]	26.08.97	06.10.97	4.3	77	72	60	-	34	47	1	52

[a]Flood event number (ID); peak discharge (Q_p); number of tracers found after the event (N_t); number of found tracers which were also found after the previous event (N_{EvB}—for surveys after particle seeding N_{EvB} corresponds to N_t); number of moved particles (N_m); percentage of buried particles (P_b) based on N_t; total recovery rate (P_t); event based recovery rate (P_{EvB}); re-emergence rate (P_{RER}—percentage of particles not found during the event but which appeared in subsequent events); percentage of lost particles after a transport event (P_{Lost}). For further details see text. Dates are formatted as day.month.year. Selected events for further analysis are in boldface.
[b]First surveys after particle seeding.
[c]Additional 127 particles were seeded.
[d]Excluded from further analysis because observation period too long or covers multiple flood events.
[e]Excluded because of poor data quality ($N_m < 10$ and $P_{Lost} > 40\%$).
[f]Includes tracers from the 2009 campaign for which the transport distance cannot be assigned to event 8.

because estimating reach-averaged flow depth is difficult in steep mountain streams. Stream power per unit area (ω, in W/m^2) is derived from discharge (Q) measurements and is defined as

$$\omega = \frac{\rho g\, QS}{w} \tag{1}$$

where ρ is the fluid density [kg/m^3], g is the acceleration due to gravity [m/s^2], S is the channel slope [m/m], and w is the flow width [m].

Tracer transport distances, sediment volumes and the depth of the active layer are expressed in this study through functional relationships with the peak stream power (the unit excess stream power $\omega_p - \omega_c$ in W/m^2 [see also *Hassan and Church*, 1992] at the peak discharge Q_p) and also with the cumulated stream power values per flood event, i.e., the sum of unit excess stream power values over the entire flood event $\Sigma(\omega - \omega_c)$ which we term the "cumulative stream energy" in J/m^2. Because the discharge measurements at the Erlenbach are conducted at 1 min time steps, we multiplied the 1 min values by 60 s for the cumulative values. The critical stream power ω_c defining the initiation of motion is based on a critical discharge of 0.48 m^3/s for the Erlenbach [*Turowski et al.*, 2011] and a critical discharge of 0.65 m^3/s for Rio Cordon [*Lenzi*, 2004].

Functional relationships between stream power, bed load transport, and tracer transport distances were derived using functional analysis on log-transformed values (for more details, see *Mark and Church* [1977]), because we expect errors in both the independent variable (stream power) and the dependent variables (bed load, transport distance, active layer depth). Simplifying the analysis, we have assumed that the errors in the x and y directions are equal. This is justified because we generally have strong correlations, and thus, the apportionment of the errors between the x and y directions has only little effect on the outcome. In addition, the fitted coefficients were corrected for log-transformation bias [*Ferguson*, 1986; *Miller*, 1984].

Figure 3. Tracer particles in the Erlenbach stream. (left) RFID campaign 2009, tracer insertion point I2. (right) RFID campaign 2010, tracer insertion point I4 (cf. Figure 1).

2.3. Estimation of Mean Transport Distances

2.3.1. Erlenbach

2.3.1.1. Tracer Particle Seeding and Recovery

In the Erlenbach, two measurement campaigns with tracer particles were completed, a magnetic tracer campaign from 1994 to 1999 and a radio frequency identification (RFID) campaign in 2009 and 2010. The magnetic tracer technique has been applied for many years to track particle movements in gravel bed streams [e.g., *Bunte and Ergenzinger*, 1989; *Gintz et al*., 1996; *Haschenburger and Church*, 1998; *Schmidt and Ergenzinger*, 1992]. RFID transponders have recently enabled the tracking of individual stones using mobile antennas in wadeable gravel bed streams [e.g., *Lamarre and Roy*, 2008; *Lamarre et al*., 2005; *Liébault et al*., 2012]. The main advantage of using passive RFID transponders instead of magnetic tracers is that they are programmable with a unique identifier (ID) and can be identified down to a depth of 0.6 m without disturbing the streambed, regardless of whether there is water, rock, wood, or mud in between [*Schneider et al*., 2010]. The term "tracer" as used in this study refers to either magnetic or RFID-tagged particles.

During the magnetic tracer campaign, in June 1994 and May 1997, a total of 313 and 227 tracer particles, respectively, was placed onto the streambed 540 m upstream of the sediment retention basin (Figure 1, location I1) [*Schwer and Rickenmann*, 1999; *Schwer et al*., 2000]. The tracers were located with a metal detector shortly after each sediment transport event whenever possible (survey periods 17 to 23, Table 2). The magnetic technique does not allow remote identification of individual particles. Buried tracers were uncovered, identified, and replaced on the streambed surface above the location where they were found.

In June 2009, 303 RFID tracers were placed onto the streambed 350 m upstream from the retention basin (Figures 1, I2; and 3). After the first transport event, 127 additional RFID tracers were placed at the same location. In May 2010, 142 RFID tracers were placed on the streambed 220 m upstream from the retention basin (Figure 1, I3), and 161 RFID tracers were placed 80 m upstream from the retention basin (Figures 1, I4; and 3). These shorter distances from the retention basin refer to a channel reach with less woody debris and therefore easier access. Thus, it was hoped to increase the tracer recovery rates, which were generally low in the Erlenbach (see section 2.3.1.2). The positions of the tracer particles on (and in) the streambed were determined with a mobile RFID antenna, directly after flood events for which bed load transport was recorded by the geophone system (survey periods 1 to 16, Table 2).

The GSD of the tracer particles corresponds to $D > D_{60B}$ of the sediment transported into the sediment retention basin, and to $D_{30Surf} < D < D_{75Surf}$ of the streambed surface material (Figure 2). A detailed description of the prepared particle size classes can be found in the supporting information (Text S1). Uncertainties introduced by the narrow GSD in determining the mean transport distances are discussed in section 2.3.1.3 and in the supporting information (Text S3).

For further analysis, we also included transport events in which the tracers were placed manually in their starting positions on the streambed; these include events 1, 2, and 8 of the RFID campaign and all events of the magnetic tracer campaign. We also neglected the fact that deeply buried particles might have been

mobilized at a later time in a future flow event [*Hassan et al*., 2013]. For simplicity, we assumed that the total transport distance of an individual grain results from multiple periods of transport and rest during a transport event and therefore was not strongly affected by the arbitrary initial particle position, once a particle is entrained. In addition, we found no differences in transport distances for events in which the tracers started from seeded positions on the streambed surface or from naturally deposited positions (see also section 3.1.3 and Figure 6).

2.3.1.2. Tracer Recovery Rates

The recovery rates of tracer particles for the individual surveys were generally low in the Erlenbach, resulting in a limited number of data points (Table 2) [see also *Schneider et al*., 2010]. These recovery rates (here called "total recovery rates" and denoted as P_t), were calculated as the ratio of total particles found (N_t) to the total number of seeded particles, and averaged roughly 30% (min 1%, max 77%) across the 23 events that were analyzed.

This paper analyzes individual events, based on changes that occurred between successive pairs of surveys (typically performed shortly after each transport event). Therefore, we determined the number of particles located during each survey that were also located during the preceding survey (N_{EvB}) and an "event-based recovery rate" (P_{EvB}), i.e., the recovery rate of particles found in two subsequent surveys ($P_{\mathrm{EvB}(i)} = 100 \cdot N_{\mathrm{EvB}(i)}/N_{t(i-1)}$)). For the first survey after particle seeding, the event-based recovery rate corresponds to the total recovery rate. Before survey 2 (Table 2), 127 additional particles were injected; thus, the event-based recovery rate of survey period 2 is based on the particles found in the previous event and the newly injected 127 particles.

To help in determining whether particles could not be found during a transport event because they were flushed out of the study reach or because they were buried at a depth outside the detection range of the antenna, we quantified the "re-emergence rate" (P_{RER}) of the tracers. The re-emergence rate refers to tracer particles that could not be found after one transport event but were known to have moved in later events, because they were found in subsequent surveys or detected immediately upstream of the retention basin using a stationary RFID antenna (as developed by *Schneider et al*. [2010]). Due to technical problems, this antenna provided no data before September 2010; however, it did detect tracers as they were flushed out of the study reach in 2011 and 2012, so we could identify these as tracer particles that had remained in the study reach during 2009 and 2010.

Finally, the "event-based percentage" of lost particles (those which either left the study reach or could not be detected anymore) was determined as $P_{\mathrm{Lost}} = 100 - P_{\mathrm{EvB}} - P_{\mathrm{RER}}$. A detailed discussion of the low recovery rates can be found in the supporting information, Text S2.

As a consequence of the low recovery rates, for the further analysis of transport distances between successive particle surveys, we selected individual flood events for which (i) more than 10 tracer particles moved and (ii) less than ~30% of particles were lost.

2.3.1.3. Mean Transport Distances of Tracer Population and Total Bed Load

We determined the mean transport distances of the tracer particles using the arithmetic mean of the individual tracer transport distances along the thalweg, considering only tracers that were known to have moved. The mean transport distance includes only tracers that moved, because later in the paper we compare this distance with the transported bed load volume, and that volume (by definition) includes only particles that moved in a given event. Using individual transport distances of tracers to estimate the mean transport distance of the bed load is problematic, because transport distance typically depends on particle size [cf. *Church and Hassan*, 1992; *Haschenburger*, 1996; *Haschenburger and Church*, 1998; *Hassan et al*., 1992; *Lenzi*, 2004; *Wilcock*, 1997] and the size distributions of the tracers and the bed load differ in two respects: (1) The mean *b* axis of the collected tracers may not always correspond to the mean b-axis of the tracer population, and (2) the tracer grain-size distribution (GSD), which ranges from 28 to 160 mm, is narrower than the average bed load GSD, which ranges from ~10 to 300 mm (Figure 2). To correct for these sampling biases, i.e., to estimate transport distances of finer and coarser grains that were not represented by the tracer particles and thus to estimate the mean transport of the bed load (Table 3), we used the empirical relation of *Church and Hassan* [1992]. The *Church and Hassan* [1992] relation was not developed for step-pool streams, but we chose this relation because it has also been tested on, and is generally supported by, field data from mountain streams [*Scheingross et al*., 2013], and on average, it fits the Erlenbach data well (see section 3.1.2).

Table 3. Bed Load and Transport Distance Characteristics for Selected Transport Events[a]

ID	Survey Date	Q_p (m^3/s)	$\omega_p - \omega_c$ (W/m^2)	$\Sigma(\omega - \omega_c)$ (J/m^2)	F_B (m^3)	f_B (m^3/m)	L_T (m)	L_B (m)	SE_{LT} (m)	SE_{LB} (m)	h_B (m)
1	18.06.09	3.0	939	5.46E + 06	75	21.6	92	120	7.6	9.8	0.20
2	07.07.09	5.0	1534	5.31E + 06	133	37.9	143	186	14.5	18.9	0.23
4	21.07.09	1.3	363	6.37E + 06	43	12.3	56	73	18.1	23.5	0.20
5	26.07.09	1.3	370	2.74E + 06	26	7.5	37	48	9.8	12.7	0.18
6	04.08.09	1.2	321	3.34E + 06	12.4	3.6	50	65	13.6	17.7	0.06
7	12.08.09	1.3	375	1.95E + 06	10.7	3.0	27	35	6.3	8.2	0.10
8	22.06.10	0.5	85	1.07E + 05	0.1	0.03	6.9	9	0.9	1.2	0.004
9	12.07.10	0.7	165	1.85E + 05	0.4	0.12	14	18	2.3	3.0	0.01
11	19.07.10	0.8	168	6.76E + 05	0.4	0.11	14	18	8.3	10.8	0.01
12	26.07.10	1.6	467	2.54E + 06	11.7	3.3	29	38.0	9.7	12.6	0.11
17	25.08.94	2.0	635	3.24E + 06	31.3	9.0	36	47	3.6	4.7	0.22
20	28.07.95	10	2852	1.45E + 07	375	107	161	209	27.4	35.6	0.57
RC1	02.10.93	4.3	662		10.2	1.7		48		23.86	0.015
RC2	30.10.93	1.7	232		1.0	0.18		5.3		4.06	0.007
RC3	12.09.94	10.4	1428		890	127		142		48.18	0.55
RC4	19.05.96	0.87	55		0.0	0.0		1.1		0.43	
RC5	15.10.96	2.96	455		57	10.96		20		11.19	0.15
RC6	12.09.98	0.96	76		0.0	0.0		1.0		0.39	
RC7	07.10.98	4.7	719		278	47.1		65		29.17	0.28

[a]Flood event number (ID); peak discharge (Q_p); unit excess stream power of peak discharge ($\omega_p - \omega_c$); cumulative unit excess stream energy ($\Sigma(\omega - \omega_c)$); total bed load volume (F_B); unit bed load volume (f_B); mean tracer transport distance (L_T); mean transport distance estimated for the total bed load (L_B = 130% of L_T). Standard error (SE_{LT}) for the mean tracer transport distances; standard error for the total transport distances of the total bed load (SE_{LB} = 130% of SE_{LT}); average active layer depth inferred from bed load volume and average transport distance (h_B). Rio Cordon events (RC1–RC7). Dates are formatted as day.month.year.

The *Church and Hassan* [1992] relation expresses the scaled transport distances (L^*) of bed load particles as a function of the scaled grain sizes:

$$L^* = L_i / L_{D50Surf} = 1.77[1 - \log_{10}(D_i / D_{50Sub})]^{1.35} \quad (2)$$

where L_i is the transport distance of individual grains of diameter D_i, $L_{D50Surf}$ is the mean transport distance of the median surface grain size (D_{50Surf}), and D_{50Sub} is the median grain size of the streambed subsurface. The use of equation (1) to estimate transport distances for unmeasured grain-size fractions is described in Text S3.

2.3.2. Rio Cordon

In Rio Cordon, the transport distances of magnetically tagged tracer stones along the stream were measured during individual snowmelt and flood events from 1993 to 1998 (Table 3) [*Lenzi*, 2004; *Lenzi et al*., 2006]. Two groups of 430 natural pebbles, cobbles, and boulders ($32 < D < 512$ mm) were painted and placed in May 1993 across two cross sections, in transverse rows with 1 to 2 m spacing. Movements of the marked clasts were mapped during repeated surveys (three transport events) from July 1993 to September 1994. Field measurements of displacement distances include the effects of a high-magnitude flood that occurred in September 1994. After this large flood, similar sets of two groups of 430 tracers were relocated on the previous two cross sections and mapped from May 1996 to October 1998 (four transport events) [*Lenzi*, 2004]. Recovered percentages of marked clasts varied from 52 to 100%, depending on the flood magnitude.

The Rio Cordon tracer population matched the bed surface grain-size distribution more closely than the Erlenbach tracer population did. Therefore, it was unnecessary to estimate the transport distances of size fractions that were not represented by the tracer particles, as we did for the Erlenbach (see section 2.3.1.3).

2.4. Bed Load Transport Measurements

2.4.1. Erlenbach: The Piezoelectric Bed Load Impact Sensors/Geophone System

Sediment transport has been monitored continuously in the Erlenbach since 1986 using piezoelectric bed load impact sensors (PBIS) and since 2000 using geophone sensors. The PBIS/Geophone system is a well-established indirect measurement method that has been used in several streams to study sediment transport. For technical details of the system, see Text S4 and *Rickenmann and McArdell* [2007], *Rickenmann et al*. [2012], *Turowski et al*. [2009], *Turowski and Rickenmann* [2011], and *Turowski et al*. [2011].

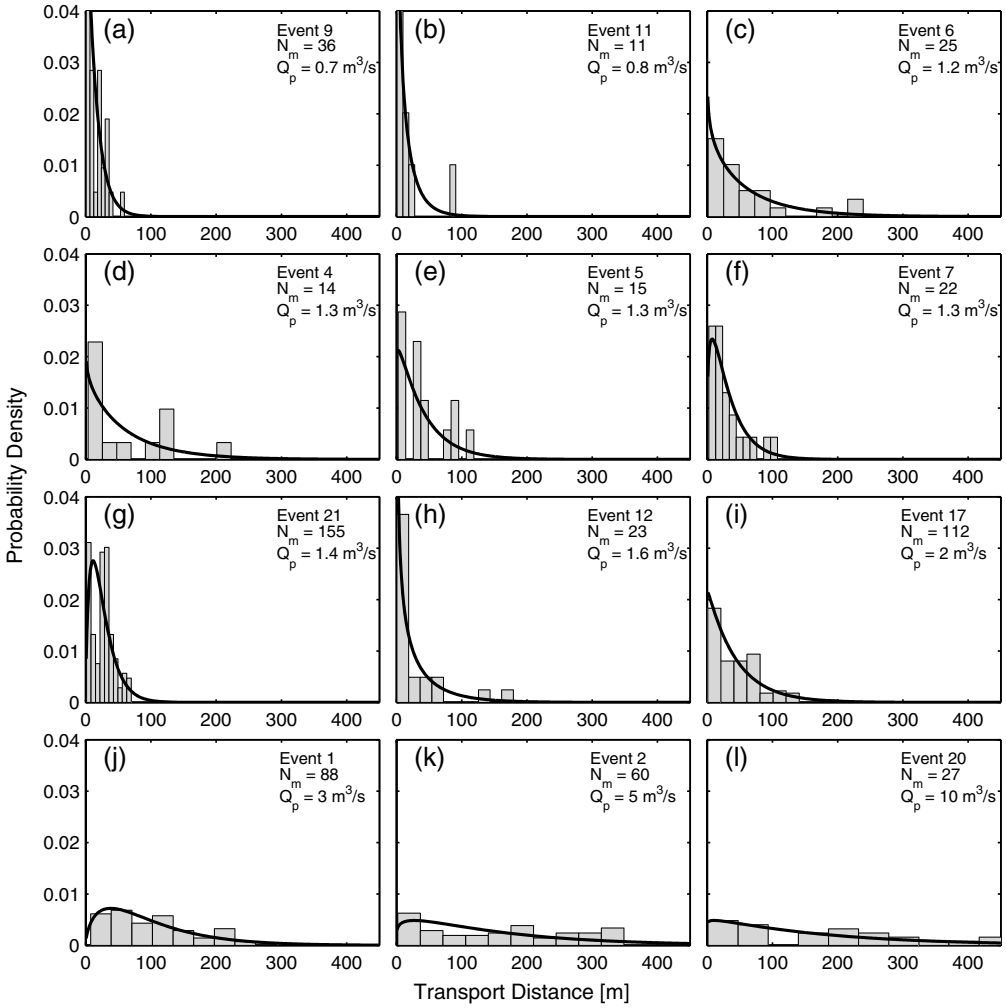

Figure 4. Tracer transport distance histograms for selected transport events sorted (a–l) according to peak discharge (Q_p), with fitted gamma distributions (heavy black lines). N_m is the number of moved tracers that the histograms are based on.

The geophone data are calibrated against sediment volumes accumulated in the retention basin (including fine material and pore volume). Therefore, we estimated bed load transport by subtracting the percentage of fine material that was likely to be transported in suspension rather than as bed load, based on the approaches of *Dade and Friend* [1998] and *Wu and Wang* [2006] (see Text S4). Based on the calibrated geophone data, we determined total bed load volumes for the transport events in which we measured tracer transport distances (Table 3). From the total bed load volumes and stream width, we estimated the bed load volume per unit width, termed "unit bed load volume".

2.4.2. Rio Cordon: Grid and Storage Basin

Sediment loads were determined by using ultrasonic sensors to survey volumetric changes in sediment deposits in the storage basin at the downstream end of the main study reach [e.g., *Lenzi et al.*, 2004]. There, an inclined grid allowed the separation of coarse sediment ($D > 20$ mm) from water and fine sediment.

3. Results

3.1. Tracer Movements

3.1.1. Influence of Flow Magnitude on the Transport Distances (Erlenbach Only)

Flow magnitude, as expressed by peak discharge, had a strong influence on the distribution of individual particles' transport distances (Figure 4). The right-hand tail of the transport distance distribution dropped off quickly for low-magnitude events (Figures 4a–4f) but was much longer for events with peak discharges larger

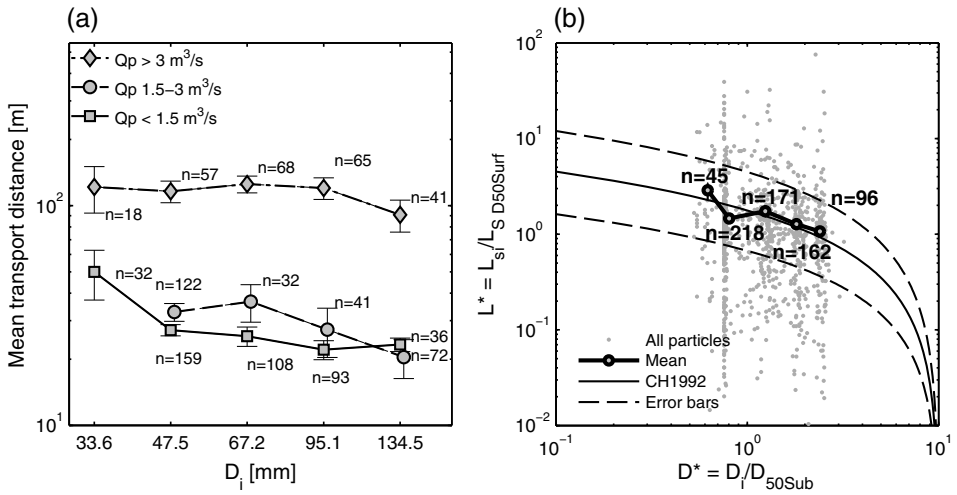

Figure 5. (a) Mean transport distances, with standard errors, for three peak discharge classes ($Q_p < 1.5\ m^3/s$, $1.5 \geq Q_p < 3\ m^3/s$, and $Q_p \geq 3\ m^3/s$), and five particle size classes indexed by their geometric means (33.6–134.5 mm), plotted as a continuous variable on a log scale. (b) Relationship between scaled travel distance (L^*) and scaled particle size (D^*) for all individual particle movements, and their medians (circles) in five grain-size classes. The transport distance L_{si} of each particle is scaled by the mean displacement of the grain-size fraction containing the D_{50Surf} of the streambed surface; D_i is scaled by the D_{50Sub} of the subsurface. The thin black line (CH1992) represents Equation (1) with the uncertainty bounds (dashed lines) given by *Church and Hassan* [1992].

than $3\ m^3/s$ (Figures 4j–4l). A gamma distribution was fitted to the tracer transport distance distribution for better visualization. The limited number of data points and the possible truncation of the distributions due to unrecovered far-moving particles (so-called "front-runners") prevent us from doing more detailed statistics on the transport distance distributions. However, the right-skewed and thin-tailed distributions that we observed, at least during low- to moderate-magnitude events, are also supported by literature results [*Hassan et al.*, 2013; *Liébault et al.*, 2012]. From these transport distance distributions, we infer that there are probably few, if any, unrecovered front-runners that would significantly change the calculated mean transport distances for low- and moderate-magnitude events. For the high-magnitude flood events with a peak discharge larger than $3\ m^3/s$, we assume that the derived mean transport distances are underestimated due to unrecovered front-runners that were flushed out of the study reach.

3.1.2. Fractional Transport Distances (Erlenbach Only)

The transport distances of individual grains were also influenced by their particle size, especially during low- and moderate-magnitude events. Figure 5a shows the average transport distances of tracer particles grouped into five logarithmic grain-size bins with centers ranging from 33.6 to 134.5 mm (spanning the tracer grain-size range 28 mm and 160 mm, respectively) and grouped into three event size classes according to peak discharge ($Q_p < 1.5\ m^3/s$, Q_p 1.5–$3\ m^3/s$, and $Q_p > 3\ m^3/s$, representing low, moderate, and high peak discharges). For the low- and moderate-magnitude events, the mean transport distance decreases with increasing particle size, whereas the transport distances during high flow events are almost unaffected by particle size (Figure 5a).

In Figure 5b, the transport distances of each individual particle (L_{si}) are shown, scaled by the transport distance L_{sD50} of the size fraction that contains the median surface grain size D_{50Surf}; these scaled transport distances are compared to scaled grain sizes (D_i scaled by the median grain size D_{50Sub} of the streambed subsurface). There is obvious scatter in the individual scaled transport distances, but their medians (Figure 5b) generally follow the pattern of the *Church and Hassan* [1992] equation (equation (1)). This justifies using equation (1) to estimate fractional transport distances from measured tracer transport distances. From the *Church and Hassan* [1992] equation, we estimated that the uncertainty in the mean transport distance due to unrepresentatively sampled grain sizes within the tracer population is smaller than 10% of the mean observed transport distance (see also Text S3). From the mean transport distances of the tracer population (L_T) and the tracer and bed load grain-size distributions (Figure 2), we estimated the mean transport distance (L_B) of the total bed load (F_B) to be 30% higher than the mean tracer transport

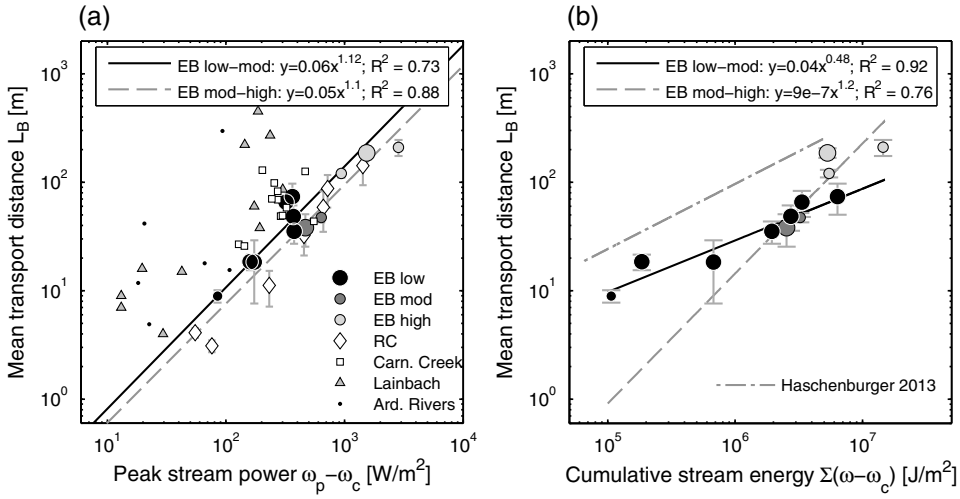

Figure 6. Mean transport distances (L_B), related to (a) the excess stream power of the peak discharge and (b) the cumulative excess stream energy over each entire flood event. Black, dark gray, and light gray circles indicate survey periods with low, moderate, and high peak discharges (Q_p) at the Erlenbach (EB) (low: $Q_p < 1.5\ m^3/s$; mod: $1.5 \geq Q_p < 3\ m^3/s$; high: $Q_p \geq 3\ m^3/s$). Small symbols show initial displacements after particle seeding; large symbols show subsequent displacements from "natural" positions for the Erlenbach. Error bars indicate standard errors. The black regression line is derived from functional analysis fitted to the low- to moderate-magnitude events, corrected for log-transformation bias. The dashed gray regression line is fitted to moderate- to high-magnitude events using the same methods. In Figure 6a, mean transport distances at Rio Cordon (RC), Carnation Creek [*Haschenburger and Church*, 1998], the Lainbach [*Gintz et al*., 1996] and for several Ardennian Rivers (Ard. Rivers) [*Houbrechts et al*., 2012] are also shown. In Figure 6b, the relation of *Haschenburger* [2013] for the Carnation Creek is added.

distance (equations (1), (S2b), and (S2c) and Text S3). The difference in transport distances arises primarily from the finer grain sizes (with generally longer transport distances) that make up a substantial proportion of the total bed load but are absent from the tracer particle distribution.

3.1.3. Scaling Mean Transport Distance With Stream Power/Energy

The mean transport distance (L_B) of the low- to moderate-magnitude events scaled roughly linearly with the excess stream power at peak discharge (Figure 6 and Table 4), and, with a somewhat stronger correlation, L_B scaled roughly as the square root of the cumulative excess stream energy (Figure 6b). In addition to the low- to moderate-magnitude events (those with a peak discharge $< 3\ m^3/s$), the high-magnitude flood events (those with a peak discharge $> 3\ m^3/s$) are also shown (light gray circles in Figure 6). The transport distances of the low-, moderate-, and high-magnitude events exhibit a consistent scaling relationship with peak stream power, with a slope of approximately 1 (Figure 6a). As a function of cumulative stream energy (Figure 6b), transport distances for these high-magnitude events plot somewhat above the regression line of the low- to moderate-magnitude events, resulting in a significantly steeper scaling exponent for the fitted moderate- to high-magnitude events. (Note also that the transport distances during the high-magnitude events may be underestimated due to unrecovered front-runners).

As a function of peak stream power, transport distances for the low-magnitude events at the Rio Cordon lie somewhat below the Erlenbach regression line, and the general trend appears to be slightly steeper (Figure 6a and Table 4). Compared to literature results, the transport distances observed at the Erlenbach and Rio Cordon are shorter than those observed at the Lainbach, Germany [*Gintz et al*., 1996], Carnation Creek, Canada [*Haschenburger*, 2013; *Haschenburger and Church*, 1998], and several Ardennian Rivers, Belgium [*Houbrechts et al*., 2012] (Figure 6), which all have gentler channel gradients. For more details on the literature data and its treatment, see Text S5 and Table S1.

Although the transport distances of the Erlenbach and the Rio Cordon tend to be generally lower compared to the literature results, the slopes of the Erlenbach and Rio Cordon regression lines in Figures 6a and 6b are in a similar range as most of the power law slopes fitted for other streams (Table 4). Only for the Ardennian River data set, which includes data from different streams, is the fitted power law characterized by a lower exponent (but also a lower r^2).

Table 4. Fitted Power Laws ($y = \alpha x^{\beta}$)

		α	β	r^2	α	β	r^2
	Data Set[a]	x = Peak Stream Power			x = Cumulative Stream Energy		
y = Transport distance	EB low-mod	0.06	1.12	0.73	0.04	0.48	0.92
	EB mod-high	0.05	1.1	0.88	9.0E-7	1.2	0.76
	EB all	0.14	0.97	0.88	0.01	0.63	0.85
	RC	0.02	1.25	0.96	0.00	0.00	0.00
	Carn. Creek	0.005	1.72	0.18	0.024[b]	0.61[b]	0.99[b]
	Lainbach	0.14	1.37	0.70			
	Ard. Rivers	8.61	0.45	0.11			
y = Unit bed load volume	EB low-mod	5.7E-10	3.85	0.88	1.1E-10	1.65	0.92
	EB mod-high	4.6E-05	1.87	0.97	4.1E-13	2.04	0.91
	EB all	2.3E-07	2.75	0.86	2.1E-11	1.78	0.93
	RC	3.3E-12	4.55	0.78			
	Ard. Rivers	5.7E-03	2.01	0.24			
y = Active layer	EB low-mod	1.3E-08	2.69	0.89	4.1E-09	1.16	0.87
	EB mod-high	7.6E-04	0.83	0.82	2.3E-07	0.89	0.87
	EB all	1.8E-06	1.77	0.78	6.1E-09	1.13	0.91
	RC	2.6E-11	3.52	0.58			
	Carn. Creek	6.7E-05	1.29	0.63			
	Ard. Rivers	7.2E-03	0.39	0.42			
		x = Mean Transport Distance					
y = Unit bed load volume	EB low-mod	8.7E-06	3.44	0.91			
	EB mod-high	7.2E-03	1.74	0.91			
	EB all	7.3E-5	2.77	0.91			
	RC	1.1E-04	3.00	0.81			
	Ard. Rivers	8.1E-04	1.93	0.81			

[a]EB: Erlenbach; RC: Rio Cordon; Carn. Creek: Carnation Creek [*Haschenburger*, 2013; *Haschenburger and Church*, 1998]; Lainbach [*Gintz et al.*, 1996]; Ard. Rivers: Ardennian Rivers [*Houbrechts et al.*, 2012].
[b]Total excess stream power relation (over the total stream width) based on hourly values taken from *Haschenburger* [2013] and converted to excess stream energy per unit width in J/m^2.

3.2. Scaling Unit Bed Load Volume With Stream Power/Energy

The transported unit bed load volumes of all observed transport events in the Erlenbach scale roughly as the cube of the peak stream power (Table 4). The low- to moderate-magnitude events exhibit even steeper scaling, with a power law exponent of 3.85 (Figure 7a and Table 4). The unit bed load volumes scale roughly as the

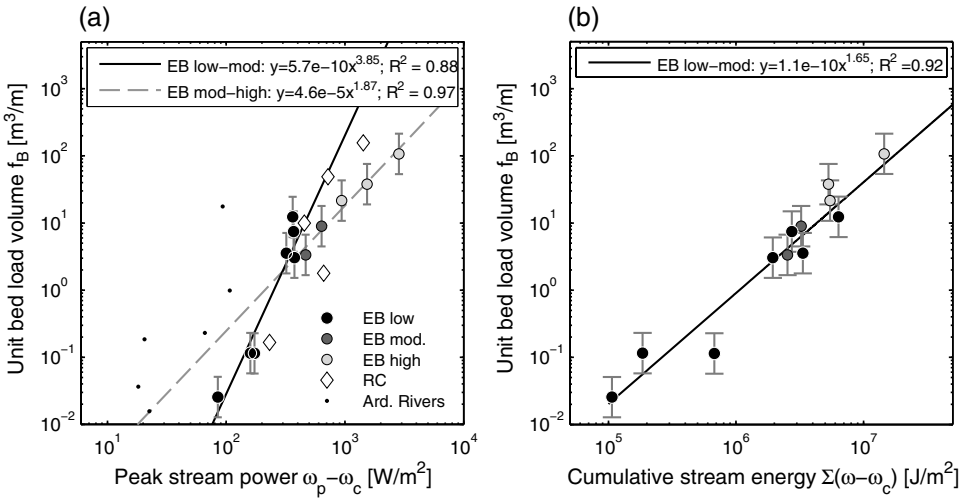

Figure 7. Unit bed load volumes (f_B) of the Erlenbach (EB), Rio Cordon (RC) and the Ardennian rivers (Ard. Rivers) related to (a) the excess stream power of the peak discharge and (b) the cumulative excess stream energy over each entire flood event. Black, dark gray and light gray circles indicate survey periods with low, moderate, and high peak discharges (Q_p) at the Erlenbach. EB errors for F_B are assumed to be a factor of 2 [*Rickenmann and McArdell*, 2008]. Regression lines were derived from the Erlenbach values by functional analysis.

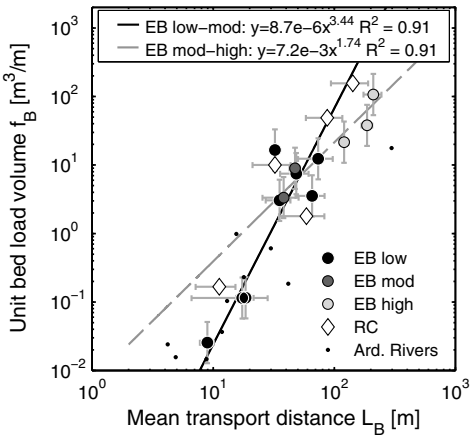

Figure 8. Unit bed load volumes (f_B) as a function of mean transport distance (L_B) for the Erlenbach (EB), Rio Cordon (RC), and the Ardennian rivers (Ard. Rivers). Black, dark gray, and light gray circles indicate events with low, moderate, and high magnitude peak discharges (Q_p) at EB. EB errors for F_B are assumed to be a factor of 2 [*Rickenmann and McArdell*, 2008] and error bars for L_B show the standard error of the transport distances. The black regression line is fitted to the EB low- to moderate-magnitude events, and the dashed gray regression line is fitted to the moderate- to high-magnitude events.

square of the cumulative stream energy (Figure 7b) for the moderate- to high-magnitude events and as a bit less than the square for the low- to moderate-magnitude events. The unit bed load volumes are more closely related to cumulative stream energy than to the peak stream power, at least for the low- to moderate-magnitude events. Unit bed load volumes of the Ardennian rivers are generally higher than those observed at the Erlenbach and Rio Cordon under comparable stream power conditions (Figure 7a).

The unit bed load volume scales roughly as the square of the mean tracer transport distance in the Ardennian Rivers, but roughly as the cube in the low- and moderate-magnitude Erlenbach events, and in Rio Cordon (Figure 8 and Table 4). For the Erlenbach, the higher-magnitude events (with peak discharges $Q_p \geq 3\ m^3/s$) plot somewhat to the right of the regression line defined by events with $Q_p < 3\ m^3/s$, although the mean transport distances are likely to be underestimated (and thus one would expect them to plot even farther to the right).

4. Discussion

Both the mean transport distances and the unit bed load volumes of our steep mountain streams, Erlenbach and Rio Cordon, are lower compared to data from other streams (Figures 6 and 7). However, their dependence on peak discharge and cumulative stream energy is broadly consistent with the patterns observed for the other streams, except for the Ardennian data set. The Ardennian data set may deviate because it consists of four different streams with only few data points per stream (one to four). This could explain the lower power law slopes and weak correlations of mean transport distances and unit bed load volumes against stream power.

The generally shorter transport distances in the Erlenbach and Rio Cordon compared the other streams for a given excess peak stream power might be explained by the different stream types. Whereas Carnation Creek and Lainbach are lower gradient mountain streams (stream gradient 0.01 m/m and 0.02 m/m, respectively) and the Ardennian data set also includes larger lowland rivers (gradients of 0.001–0.011), the mountain streams Erlenbach and Rio Cordon are characterized by steep channels (gradients of 0.17 and 0.13, respectively), step-pools, and rough bed topography. The rough bed topography might be responsible for relatively lower bed load volumes and transport distances, compared to the other sites. Bed load transport is relatively lower in steep streams compared to lowland rivers, due to a reduced transport efficiency resulting from an increased demand for particle entrainment [e.g., *Bathurst*, 2013; *Bunte et al.*, 2013; *Lamb et al.*, 2008; *Mueller et al.*, 2005] and a reduced energy available for sediment transport resulting from macro-roughness [e.g., *Bathurst et al.*, 1987; *Nitsche et al.*, 2011; *Chiari and Rickenmann*, 2011; *Yager et al.*, 2012a].

The cumulative stream energy, which represents the integrated energy of an entire flow event, has a larger dynamic range (i.e., varies over more orders of magnitude) than peak stream power does. Perhaps partly for this reason, it also appears to be somewhat better than peak stream power at explaining the variation in transport distance and unit bed load volume among low- and moderate-magnitude events at the Erlenbach (Figures 6 and 7 and Table 4). *Haschenburger* [2013] also found a very strong correlation ($r^2 = 0.99$) between mean transport distance and cumulative stream energy for Carnation Creek. However, transport distances of the high-magnitude Erlenbach events clearly deviate from the cumulative stream energy relationship defined by the low- and moderate-magnitude events (Figure 6); if the assumed underestimation of these transport distances (due to potentially unrecovered front-runners) could be corrected, this deviation would presumably be even larger.

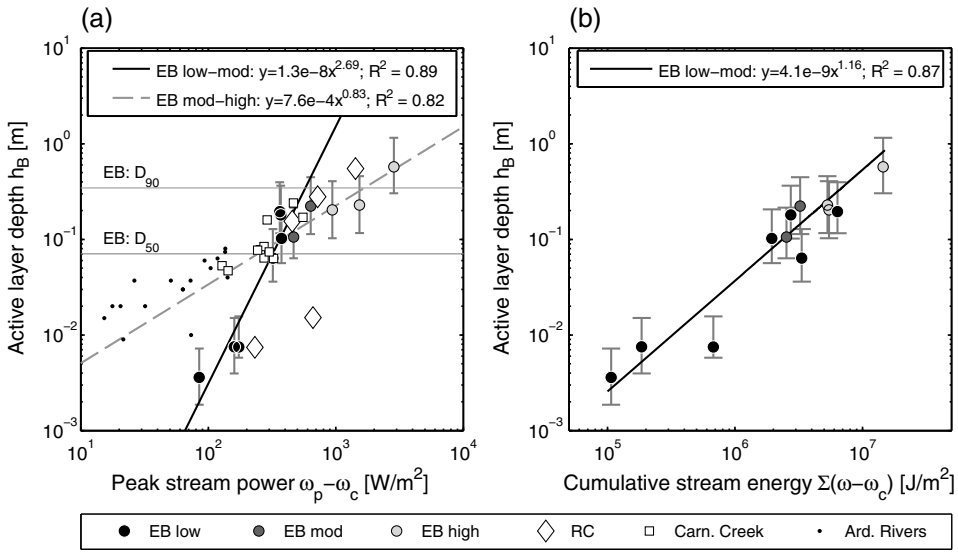

Figure 9. Back-calculated active layer depth related to (a) unit excess stream power of the peak discharge and (b) unit cumulative excess stream energy for the Erlenbach (EB) and Rio Cordon (RC). Black, dark gray, and light gray circles indicate events with low, moderate, and high peak discharges (Q_p) at the Erlenbach (EB). The solid black lines were fitted to the Erlenbach low- to moderate-magnitude events ($Q_p < 3\ m^3/s$). The dashed black line in Figure 9a was fitted to the moderate- to high-magnitude events ($Q_p \geq 1.5\ m^3/s$). Erlenbach error bars are derived from uncertainties in the measured bed load volume (factor 2) and the standard error of the transport distances. Squares represent scour chain measurements in Carnation Creek, Canada [*Haschenburger and Church*, 1998]. Small black dots (Ard. Rivers) are based on scour chain measurements in several Ardennian Rivers, Belgium [*Houbrechts et al*., 2012]. The black and dashed gray lines were not fitted to data from Rio Cordon, Carnation Creek, or the Ardennian Rivers.

4.1. Back Calculation of an Active Layer Depth

In our Erlenbach and Rio Cordon data, bed load volumes scale much more steeply than transport distances do, as functions of peak stream power (power law slopes of roughly 3 and 1, respectively). Bed load volumes also scale much more steeply with cumulative stream energy than transport distances do (power law slopes of roughly 1.8 and 0.5, respectively). These observations imply that large bed load volumes during large storms may arise primarily from deeper and wider bed scouring and only secondarily from longer transport distances. The impact of the water flow on the streambed can be discussed using the active layer concept. In this concept, as a modeling assumption, the probability distribution for a particle to be entrained by the flow is simplified to a step function dividing the sediment vertically into two layers [*Hirano*, 1971; *Parker*, 1991; *Parker et al*., 2000]: an immobile layer underlying a temporally and spatially variable near-surface active layer, in which the probability of erosion per unit time is the same for every grain. In this study we consider the active layer as a virtual layer in which all of the particles are entrained and which is mobilized over the entire stream width during the course of the transport event.

From measurements of transport distances (L_B), bed load volumes (F_B), and average stream width (w), we estimated an active layer depth (h_B), describing the flood impact on the streambed, for individual transport events (Figure 9) via the sediment continuity equation:

$$h_B = \frac{F_B}{L_B w} \tag{3}$$

The mean derived active layer thickness (h_B) that we calculated from equation (2) for the Erlenbach is about 0.01–0.22 m for the low- to moderate-magnitude events and about 0.57 m for the largest transport event observed (Table 3), which is roughly similar to the D_{90Surf} of the bed surface. Since the mean transport distances are potentially underestimated for the high-magnitude events, the back-calculated active layer depths (light gray circles, Figure 9) might be overestimated for these events. Although the high values might be somewhat overestimated, these values of the active layer depth are similar to independent measurements from the Erlenbach. Consider, for example, the active layer depth of 0.57 m inferred for event 20, which had a peak discharge of $10\ m^3/s$. For an event with a similar peak discharge ($9.3\ m^3/s$; event 15, Table 2)

preflood and postflood long-profile measurements show that the mean erosion was 0.47 m along a 600 m channel reach and the maximum local erosion was 2.8 m [*Turowski et al*., 2013]. In addition, maximum mobile grain sizes of around 0.5 m were observed in another comparable transport event [*Turowski et al*., 2009].

Inferred active layer depths in the Erlenbach scale approximately linearly with cumulative stream energy, for both large and small events (Figure 9b). The relationship between active layer depth and peak stream power, by contrast, cannot be described by a single power function over the entire range of flow magnitudes (Figure 9a). The data shown in Figure 9a indicate two trends: one relation with a power law slope of 2.7 for low-to-moderate magnitude events, and a second relation with a power law slope of 0.8 for events with moderate-to-high flow magnitudes.

The trends in active layer depth in Figure 9a are similar to those shown in Figure 7a for unit bed load volumes. Both are steep functions of peak stream power for low-to-moderate flow magnitudes and markedly shallower functions of peak stream power for moderate-to-high flow magnitudes. This shift could arise if, particularly at low or moderate flows, only a fraction of the channel width actively transports sediment [*Dietrich et al*., 1989], and if this active layer width increases with increasing flow. Thus, at low-to-moderate flows, the active layer width, active layer depth, and average transport distance may all increase with increasing flow, with the result that bed load transport is a steep function of flow magnitude. One may further hypothesize that in moderate and larger events, the active layer width reaches both banks and thus cannot increase farther; thus, only active layer depth and transport distance can continue to increase, making bed load transport a shallower function of stream power in this magnitude range.

To understand how this hypothesized mechanism might affect the active layer depths shown in Figure 9a, one must remember that these are virtual quantities averaged over the entire channel width. They represent the actual active layer depth, times the ratio between the actual active layer width and the channel width. Thus, the inferred active layer depth would reflect the increase in the real-world width and depth of the active layer in the low-to-moderate magnitude range (and thus be a relatively steep function of stream power), but only the increase in real-world depth of the active layer at higher flow magnitudes (where the real-world active layer width has maxed out at the full width of the channel).

Although the total active layer depth in the Erlenbach can be related to both cumulative stream energy and peak stream power (Figure 9), peak stream power provides a basis for comparison with other field observations, namely, at Rio Cordon, Carnation Creek [*Haschenburger and Church*, 1998], and the Ardennnian Rivers [*Houbrechts et al*., 2012], where cumulative stream energy could not be estimated. The estimated active layer depths at Rio Cordon (white diamonds, Figure 9a) follow a similar trend to the Erlenbach observations during moderate-high flow magnitudes (solid black circles, Figure 9a), although with more scatter. The two very low active layer depth values obtained in Rio Cordon, lying below the Erlenbach trend lines (Figure 9a), were observed under supply-limited conditions before the September 1994 flood event as reported by *Lenzi* [2004]. The 1994 flood was an exceptional event which broke up the stable bed structures and led to almost unlimited sediment supply [*Lenzi et al*., 2004]. The bed load volumes (and thus active layer depths) observed at Rio Cordon are markedly larger after this extreme flood event.

The Ardennian and Carnation Creek active layer depths shown in Figure 9a were measured by scour chains. They follow a similar trend as the Erlenbach back-calculated active layer depths for moderate-high flow magnitudes but lie well above the Erlenbach values for low-magnitude stream flow magnitudes. The smaller active layer depths in the Erlenbach compared to the Ardennian Rivers and Carnation Creek during low-magnitude flow conditions (Figure 9a) might be explained by the bed configuration of steep mountain streams with more stable bed structure (form and grain roughness, bedrock, woody debris), and a more limited sediment supply, compared to lower gradient streams. Alternatively, the smaller inferred active layer depth in the Erlenbach may be an artifact of changes in the width of the active layer, as outlined in the hypothesis above. A third possible explanation might be the different measurement techniques used. Our back-calculation methods average the active layer depth over space and time, whereas scour chains measure a spatially local, and temporally maximal, active layer depth for a given transport event.

5. Conclusions

We have presented measurements of bed load transport volumes and transport distances of tracer particles of two steep mountain streams, the Erlenbach (Switzerland) and Rio Cordon (Italy). Despite low tracer recovery

rates at the Erlenbach (particularly for large events) and the resulting limited number of data points (Table 2), the observed transport distances and unit bed load volumes were strongly correlated to both the peak stream power and the cumulative stream energy (Figures 6 and 7) of individual transport events.

Both the Erlenbach and Rio Cordon are characterized by shorter transport distances and smaller unit bed load volumes than those observed in several lower gradient streams (Figures 6 and 7). However, transport distance and unit bed load volumes in all of these streams exhibit broadly similar scaling with peak stream power (Table 4), implying that these scaling relationships are not strongly dependent on stream gradient.

Unit bed load volumes scale much more steeply than tracer transport distances do, as functions of either stream power or cumulative stream energy (Figures 6 and 7). Furthermore, unit bed load volumes scale as roughly the third power of transport distances (Figure 8). These observations imply that storm-to-storm variations in bed load volumes arise predominantly through variations in scour depth and width rather than through variations in transport distances. From the observed bed load volumes and transport distances, we back-calculated an effective mean active layer depth, which also was strongly correlated with both peak stream power and cumulative stream energy (Figure 9) and was broadly consistent with independent measurements of scour depth.

Approximating bed load transport in steep, rough mountain streams by a continuous, uniform active layer involves gross simplifications, which will be challenged by (i) partial sediment transport [*Wilcock and McArdell*, 1997], (ii) mobile and stationary zones of the streambed [e.g., *Hassan et al*., 2005; *Marquis and Roy*, 2012; *Yager et al*., 2012b], (iii) variations in the horizontal and vertical dimensions of the active layer over time [e.g., *Haschenburger*, 1996; *Hassan*, 1990; *Wilcock et al*., 1996], and (iv) variations in the fraction of the channel width that is actively transporting sediment [*Dietrich et al*., 1989]. Despite these obvious limitations, the active layer concept provides a useful simplified characterization of streambed response to hydraulic forcing during bed load transport. Independent, direct measurements of active layer depths in steep streams would be helpful for interpreting the active layer depths results derived from the back-calculation procedure presented here.

Acknowledgments
This study was supported by CCES project APUNCH and SNF grant 200021_124634/1, the Swiss Federal Research Institute WSL, and the Swiss Federal Institute of Technology ETH. We thank K. Bunte for providing the Erlenbach grain-size distribution data. We thank A. Badoux, B. J. MacVicar, the Editor, and several anonymous reviewers for their constructive remarks on the manuscript.

References

Badoux, A., N. Andres, and J. M. Turowski (2014), Damage costs due to bedload transport processes in Switzerland, *Nat. Hazards Earth Syst. Sci.*, *14*, 279–294, doi:10.5194/nhess-14-279-2014.

Bagnold, R. A. (1966), *An Approach to the Sediment Transport Problem From General Physics*, U.S. Geological Survey Professional Paper 422–1, pp. 37, U.S. Government Printing Office, Washington.

Bathurst, J. C. (2013), Critical conditions for particle motion in coarse bed materials of nonuniform size distribution, *Geomorphology*, *197*(0), doi:10.1016/j.geomorph.2013.05.008.

Bathurst, J. C., W. H. Graf, and H. H. Cao (1987), *Bed Load Discharge Equations for Steep Mountain Rivers*, Wiley, New York.

Bradley, N. D., and G. E. Tucker (2012), Measuring gravel transport and dispersion in a mountain river using passive radio tracers, *Earth Surf. Processes Landforms*, *37*(10), 1023–1132, doi:10.1002/esp.3223.

Bunte, K., and S. R. Abt (2001a), Sampling frame for improving pebble count accuracy in coarse gravel bed streams, *J. Am. Water Resour. Assoc.*, *37*(4), 1001–1014, doi:10.1111/j.1752-1688.2001.tb05528.x.

Bunte, K., and S. R. Abt (2001b), *Sampling Surface and Subsurface Particle-Size Distributions in Wadeable Gravel and Cobble-Bed Streams for Analyses in Sediment Transport, Hydraulics, and Streambed Monitoring*, pp. 428, U.S. Department of Agriculture, Forest Service, Fort Collins, CO.

Bunte, K., and P. Ergenzinger (1989), New tracer techniques for particles in gravel bed rivers, *Bull. Societe Geographique de Liege*, *25*, 85–90.

Bunte, K., S. R. Abt, J. P. Potyondy, and S. E. Ryan (2004), Measurement of coarse gravel and cobble transport using portable bedload traps, *J. Hydraul. Eng.-Asce*, *130*(9), 879–893, doi:10.1061/(asce)0733-9429(2004)130:9(879.

Bunte, K., S. R. Abt, J. P. Potyondy, and K. W. Swingle (2009), Comparison of three pebble count protocols (EMAP, PIBO, and SFT) in two mountain gravel-bed streams, *J. Am. Water Resour. Assoc.*, *45*(5), 1209–1227, doi:10.1111/j.1752-1688.2009.00355.x.

Bunte, K., S. R. Abt, K. W. Swingle, D. A. Cenderelli, and J. M. Schneider (2013), Critical shields values in coarse-bedded steep streams, *Water Resour. Res.*, *49*, 7427–7447, doi:10.1002/2012WR012672.

Chiari, M., and D. Rickenmann (2011), Back-calculation of bedload transport in steep channels with a numerical model, *Earth Surf. Processes Landforms*, *36*(6), 805–815, doi:10.1002/esp.2108.

Church, M., and M. A. Hassan (1992), Size and distance of travel of unconstrained clasts on a streambed, *Water Resour. Res.*, *28*(1), 299–303, doi:10.1029/91WR02523.

Dade, W. B., and P. F. Friend (1998), Grain-size, sediment-transport regime, and channel slope in alluvial rivers, *J. Geol.*, *106*(6), 661–675, doi:10.1086/516052.

Dietrich, W. E., J. W. Kirchner, H. Ikeda, and F. Iseya (1989), Sediment supply and the development of the coarse surface layer in gravel-bedded rivers, *Nature*, *340*(6230), 215–217.

Einstein, H. A. (1937), The bed load transport as probability problem, PhD thesis, Mitteilung der Versuchsanstalt fuer Wasserbau, Eidgenössische Technische Hochschule, Zurich, Rascher, Zürich, Switzerland.

Ferguson, R. I. (1986), River loads underestimated by rating curves, *Water Resour. Res.*, *22*(1), 74–76, doi:10.1029/WR022i001p00074.

Gintz, D., M. A. Hassan, and K.–. H. Schmidt (1996), Frequency and magnitude of bedload transport in a mountain river, *Earth Surf. Processes Landforms*, *21*(5), 433–445, doi:10.1002/(sici)1096-9837(199605)21:5<433::aid-esp580>3.0.co;2-p.

Gomez, B., and M. Church (1989), An assessment of bed load sediment transport formulae for gravel bed rivers, *Water Resour. Res.*, *25*(6), 1161–1186.

Haschenburger, J. K. (1996), Scour and fill in a gravel-bed channel: Observations and stochastic models, PhD thesis, University of British Columbia, Vancouver.
Haschenburger, J. K. (2013), Tracing river gravels: Insights into dispersion from a long-term field experiment, *Geomorphology*, *200*(0), doi:10.1016/j.geomorph.2013.03.033.
Haschenburger, J. K., and M. Church (1998), Bed material transport estimated from the virtual velocity of sediment, *Earth Surf. Processes Landforms*, *23*(9), 791–808, doi:10.1002/(SICI)1096-9837(199809)23:9<791::AID-ESP888>3.0.CO;2-X.
Hassan, M. A. (1990), Scour, fill, and burial depth of coarse material in gravel bed streams, *Earth Surf. Processes Landforms*, *15*(4), 341–356, doi:10.1002/esp.3290150405.
Hassan, M. A., and M. Church (1992), The movement of individual grains on the streambed, paper presented at 3RD workshop on Dynamics of Gravel-Bed Rivers, edited by P. Billi, R. D. Hey, and C. R. Thorne, John Wiley, Florence, Italy.
Hassan, M. A., and P. Ergenzinger (2005), Use of tracers in fluvial geomorphology, in *Tools in Fluvial Geomorphology*, edited by G. M. Kondolf and H. Piégay, John Wiley, Chichester, UK, doi:10.1002/0470868333.ch14.
Hassan, M. A., M. Church, and A. P. Schick (1991), Distance of movement of coarse particles in gravel bed streams, *Water Resour. Res.*, *27*(4), 503–511, doi:10.1029/90WR02762.
Hassan, M. A., M. Church, and P. J. Ashworth (1992), Virtual rate and mean distance of travel of individual clasts in gravel-bed channels, *Earth Surf. Processes Landforms*, *17*(6), 617–627, doi:10.1002/esp.3290170607.
Hassan, M. A., M. Church, T. E. Lisle, F. Brardinoni, L. Benda, and G. E. Grant (2005), Sediment transport and channel morphology of small, forested streams, *J. Am. Water Resour. Assoc.*, *41*(4), 853–876.
Hassan, M. A., H. Voepel, R. Schumer, G. Parker, and L. Fraccarollo (2013), Displacement characteristics of coarse fluvial bed sediment, *J. Geophys. Res. Earth Surface*, *118*, 155–165, doi:10.1029/2012JF002374.
Helley, E. J., and W. Smith (1971), *Development and Calibration of a Pressure-Difference Bedload Sampler*, pp. 18 , U.S. Dept. of the Interior, Geological Survey, Water Resources Division, Menlo Park, Calif.
Hirano, M. (1971), River bed degradation with armouring [in Japanese], *Trans. Jpn. Soc. Civ. Eng.*, *3*(2), 194–195.
Houbrechts, G., J. Van Campenhout, Y. Levecq, E. Hallot, A. Peeters, and F. Petit (2012), Comparison of methods for quantifying active layer dynamics and bedload discharge in armoured gravel-bed rivers, *Earth Surf. Processes Landforms*, doi:10.1002/esp.3258.
Klingeman, P. C. (1979), *Sediment Transport Research Facilities, Oak Creek*, Water Resources Research Institute, Oregon State University, Corvallis, OregonRep.
Lajeunesse, E., L. Malverti, and F. Charru (2010), Bed load transport in turbulent flow at the grain scale: Experiments and modeling, *J. Geophys. Res.*, *115*, F04001, doi:10.1029/2009JF001628.
Lamarre, H., and A. G. Roy (2008), The role of morphology on the displacement of particles in a step-pool river system, *Geomorphology*, *99*(1–4), 270–279, doi:10.1016/j.geomorph.2007.11.005.
Lamarre, H., B. MacVicar, and A. G. Roy (2005), Using passive integrated transponder (PIT) tags to investigate sediment transport in gravel-bed rivers, *J. Sediment. Res.*, *75*(4), 736–741, doi:10.2110/jsr.2005.059.
Lamb, M. P., W. E. Dietrich, and J. G. Venditti (2008), Is the critical Shields stress for incipient sediment motion dependent on channel-bed slope?, *J. Geophys. Res.*, *113*, F02008, doi:10.1029/2007JF000831.
Laronne, J. B., D. N. Outhet, J. L. Duckham, and T. J. McCabe (1992), *Determining Event Bedload Volumes for Evaluation of Potential Degradation Sites Due To Gravel Extraction, N.S.W., Australia*, pp. 87–94, International Association of Hydrological Sciences, Wallingford, Oxfordshire.
Lenzi, M. A. (2004), Displacement and transport of marked pebbles, cobbles and boulders during floods in a steep mountain stream, *Hydrol. Processes*, *18*(10), 1899–1914, doi:10.1002/hyp.1456.
Lenzi, M. A., L. Mao, and F. Comiti (2004), Magnitude-frequency analysis of bed load data in an Alpine boulder bed stream, *Water Resour. Res.*, *40*, W07201, doi:10.1029/2003WR002961.
Lenzi, M. A., L. Mao, and F. Comiti (2006), When does bedload transport begin in steep boulder-bed streams?, *Hydrol. Processes*, *20*(16), 3517–3533, doi:10.1002/hyp.6168.
Liébault, F., and J. B. Laronne (2008), Evaluation of bedload yield in gravel-bed rivers using scour chains and painted tracers: The case of the Esconavette Torrent (Southern French Prealps), *Geodinamica Acta*, *21*(1–2), 23–34, doi:10.3166/ga.21.23-34.
Liébault, F., H. Bellot, M. Chapuis, S. Klotz, and M. Deschâtres (2012), Bedload tracing in a high-sediment-load mountain stream, *Earth Surf. Processes Landforms*, doi:10.1002/esp.2245.
Liechti, K. (2008), Starke Gewitter im Juni 2007—Einordnung und Hydrologische Modellierung für die Regionen Huttwil (BE) und Einsiedeln (SZ), Master thesis, 107 pp., University of Zurich and Swiss Federal Research Institute WSL, Zurich.
Mao, L., M. Cavalli, F. Comiti, L. Marchi, M. A. Lenzi, and M. Arattano (2009), Sediment transfer processes in two Alpine catchments of contrasting morphological settings, *J. Hydrol.*, *364*(1–2), 88–98, doi:10.1016/j.jhydrol.2008.10.021.
Mao, L., F. Comiti, and M. Lenzi (2010), Bedload dynamics in steep mountain rivers: Insights from the Rio Cordon Experimental Station (Italian Alps), in *Bedload-Surrogate Monitoring Technologies*, edited by J. R. Gray, J. B. Laronne, and J. D. G. Marr, U.S. Geol. Surv. Sci. Investig. Rpt. 2010–5091, 253–265 pp. [Available at http://pubs.usgs.gov/sir/2010/5091/papers/listofpapers.html.]
Mark, D., and M. Church (1977), On the misuse of regression in earth science, *J. Int. Assoc. Math. Geol.*, *9*(1), 63–75, doi:10.1007/bf02312496.
Marquis, G. A., and A. G. Roy (2012), Using multiple bed load measurements: Toward the identification of bed dilation and contraction in gravel-bed rivers, *J. Geophys. Res.*, *117*, F01014, doi:10.1029/2011JF002120.
Miller, D. M. (1984), Reducing transformation bias in curve fitting, *Am. Statistician*, *38*(2), 124–126, doi:10.2307/2683247.
Molnar, P., A. L. Densmore, B. W. McArdell, J. M. Turowski, and P. Burlando (2010), Analysis of changes in the step-pool morphology and channel profile of a steep mountain stream following a large flood, *Geomorphology*, *124*, 85–94, doi:10.1016/j.geomorph.2010.08.014.
Mueller, E. R., J. Pitlick, and J. M. Nelson (2005), Variation in the reference shields stress for bed load transport in gravel-bed streams and rivers, *Water Resour. Res.*, *41*(4W04006), doi:10.1029/2004WR003692.
Nitsche, M., D. Rickenmann, J. M. Turowski, A. Badoux, and J. W. Kirchner (2011), Evaluation of bedload transport predictions using flow resistance equations to account for macro-roughness in steep mountain streams, *Water Resour. Res.*, *47*, W08513, doi:10.1029/2011WR010645.
Parker, G. (1991), Selective sorting and abrasion of river gravel. I: Theory, *J. Hydraul. Eng.-ASCE*, *117*(2), 131–149, doi:10.1061/(asce)0733-9429(1991)117:2(131.
Parker, G., C. Paola, and S. Leclair (2000), Probabilistic Exner sediment continuity equation for mixtures with no active layer, *J. Hydraul. Eng.-ASCE*, *126*(11), 818–826, doi:10.1061/(asce)0733-9429(2000)126:11(818.
Reid, I., J. T. Layman, and L. E. Frostick (1980), The continuous measurement of bedload discharge, *J. Hydraul. Res.*, *18*(3), 243–249, doi:10.1080/00221688009499550.
Rickenmann, D. (2001), Comparison of bed load transport in torrents and gravel bed streams, *Water Resour. Res.*, *37*(12), 3295–3305, doi:10.1029/2001WR000319.

Rickenmann, D., and B. W. McArdell (2007), Continuous measurement of sediment transport in the Erlenbach stream using piezoelectric bedload impact sensors, *Earth Surf. Processes Landforms*, *32*(9), 1362–1378, doi:10.1002/esp.1478.

Rickenmann, D., and B. W. McArdell (2008), Calibration of piezoelectric bedload impact sensors in the Pitzbach mountain stream, *Geodinamica Acta*, *21*(1–2), 35–52, doi:10.3166/ga.21.35-52.

Rickenmann, D., J. M. Turowski, B. Fritschi, A. Klaiber, and A. Ludwig (2012), Improved sediment transport measurements in the Erlenbach stream including a moving basket system, *Earth Surf. Processes Landforms*, *37*, 1000–1011, doi:10.1002/esp.3225.

Sayre, W. W., and D. W. Hubbell (1964), *Transport and Dispersion of Labeled Bed Material, North Loup River, Nebraska: Transport of Radionuclides by Streams*, Geological Survey, Washington.

Scheingross, J. S., E. W. Winchell, M. P. Lamb, and W. E. Dietrich (2013), Influence of bed patchiness, slope, grain hiding, and form drag on gravel mobilization in very steep streams, *J. Geophys. Res. Earth Surface*, *118*, 982–1001, doi:10.1002/jgrf.20067.

Schmidt, K.-H., and P. Ergenzinger (1992), Bedload entrainment, travel lengths, step lengths, rest periods—Studied with passive (iron, magnetic) and active (radio) tracer techniques, *Earth Surf. Processes Landforms*, *17*(2), 147–165, doi:10.1002/esp.3290170204.

Schneider, J., R. Hegglin, S. Meier, J. M. Turowski, M. Nitsche, and D. Rickenmann (2010), Studying sediment transport in mountain rivers by mobile and stationary RFID antennas, in *Proceedings of the International Conference on Fluvial Hydraulics: River Flow 2010*, edited by A. Dittrich et al., pp. 1723–1730, Bundesanstalt für Wasserbau, Braunschweig.

Schumm, S. A. (1977), *The Fluvial System*, pp. 338, Wiley, New York.

Schwer, P., and D. Rickenmann (1999), *Single Particle Movements in Steep Torrents: Observations With Magnetically Tagged Tracer Stones*, WSL, Birmensdorf, Switzerland.

Schwer, P., D. Rickenmann, and C. Hegg (2000), Beobachtungen zum Einzelkorntransport in Wildbächen, paper presented at *Beiträge zur Geomorphologie. Proceedings der Fachtagung der Schweizerischen Geomorphologischen Gesellschaft Birmensdorf, Eidgenössische Forschungsanstalt WSL*. 65–75 Bramois (Kt. Wallis) 8.-10. Juli 1999

Sear, D. A., M. W. E. Lee, R. J. Oakley, P. A. Carling, and M. B. Collins (2000), Coarse sediment tracing technology in littoral and fluvial environments: A review, in *Tracers in the Environment*, edited by F. I, pp. 21–55, Wiley, Chichester, U. K.

Turowski, J. M., and D. Rickenmann (2011), Measuring the statistics of bed-load transport using indirect sensors, *J. Hydraul. Eng.-ASCE*, *137*(1), 116–121, doi:10.1061/(asce)hy.1943-7900.0000277.

Turowski, J. M., E. M. Yager, A. Badoux, D. Rickenmann, and P. Molnar (2009), The impact of exceptional events on erosion, bedload transport and channel stability in a step-pool channel, *Earth Surf. Processes Landforms*, *34*(12), 1661–1673, doi:10.1002/Esp.1855.

Turowski, J. M., A. Badoux, and D. Rickenmann (2011), Start and end of bedload transport in gravel-bed streams, *Geophys. Res. Lett.*, *38*, L04401, doi:10.1029/2010GL046558.

Turowski, J. M., A. Badoux, J. Leuzinger, and R. Hegglin (2013), Large floods, alluvial overprint, and bedrock erosion, *Earth Surf. Processes Landforms*, *38*, 947–958, doi:10.1002/esp.3341.

Wilcock, P. R. (1997), Entrainment, displacement and transport of tracer gravels, *Earth Surf. Processes Landforms*, *22*(12), 1125–1138, doi:10.1002/(sici)1096-9837(199712)22:12<1125::aid-esp811>3.3.co;2-m.

Wilcock, P. R., and B. W. McArdell (1997), Partial transport of a sand/gravel sediment, *Water Resour. Res.*, *33*(1), 235–245, doi:10.1029/96WR02672.

Wilcock, P. R., A. F. Barta, C. C. Shea, G. M. Kondolf, W. V. G. Matthews, and J. Pitlick (1996), Observations of flow and sediment entrainment on a large gravel-bed river, *Water Resour. Res.*, *32*(9), 2897–2909, doi:10.1029/96WR01628.

Wolman, G. M. (1954), A method of sampling coarse river-bed material, *Trans. Am. Geophys. Union*, *35*(6), 951–956.

Wong, M., and G. Parker (2006), Flume experiments with tracer stones under bedload transport, paper presented at River, Coastal and Estuarine Morphodynamics: RCEM 2005, Taylor & Francis Group, London.

Wong, M., G. Parker, P. DeVries, T. M. Brown, and S. J. Burges (2007), Experiments on dispersion of tracer stones under lower-regime plane-bed equilibrium bed load transport, *Water Resour. Res.*, *43*, W03440, doi:10.1029/2006WR005172.

Wu, W., and S. Wang (2006), Formulas for sediment porosity and settling velocity, *J. Hydraul. Eng.*, *132*(8), 858–862, doi:10.1061/(ASCE)0733-9429(2006)132:8(858).

Yager, E. M., W. E. Dietrich, J. W. Kirchner, and B. W. McArdell (2012a), Prediction of sediment transport in step-pool channels, *Water Resour. Res.*, *48*, W01541, doi:10.1029/2011WR010829.

Yager, E. M., W. E. Dietrich, J. W. Kirchner, and B. W. McArdell (2012b), Patch dynamics and stability in steep, rough streams, *J. Geophys. Res.*, *117*, F02010, doi:10.1029/2011JF002253.